Dalton Transactions

ROYAL SOCIETY OF CHEMISTRY

COMMUNICATION

Cite this: *Dalton Trans.*, 2023, **52**, 12198

Received 7th July 2023,
Accepted 13th August 2023

DOI: 10.1039/d3dt02134c

rsc.li/dalton

Linker engineering toward near-infrared-I emissive metal–organic frameworks for amine detection†

Hai-Lun Xia, Kang Zhou, Lei Wang, Jian Zhang* and Xiao-Yuan Liu *

Herein, organic linker-based near-infrared-I (NIR-I) emissive metal–organic frameworks (MOFs), with a maximum emission peak at 741 nm, were synthesized *via* linker engineering. By integration of stronger acceptor and donor groups into one linker, a significant bathochromic-shift is realized. This MOF exhibits great selectivity and sensitivity for aniline and *p*-phenylenediamine detection. This finding provides new insights into the rational design of NIR-MOFs for sensing and related applications.

Organic linker-based luminescent metal–organic frameworks (LMOFs) have shown potential applications in solid-state-light,[1–5] sensing[6–12] and bioimaging[13–15] owing to the tunable linker structures and highly accessible functional sites.[16] While the emission wavelength of LMOFs is almost limited in the visible light range, and there is lack of studies on organic linker-based near-infrared emissive MOFs (NIR-MOFs), the major challenge is to design and synthesize organic linkers with NIR emission. In recent years, NIR emissive molecules with emission wavelength in the 650–1700 nm range, such as benzo[1,2-*c*:4,5-*c*′]bis([1,2,5]thiadiazole) and its derivative based compounds,[17–22] have been extensively studied, especially for bioimaging and biosensing, due to their high spatiotemporal resolution, improved penetration depth and non-invasiveness. To realize NIR emission, the organic compounds are designed with large conjugated backbones, which usually suffer from low quantum efficiency due to the strong intermolecular interactions and aggregation-caused quenching (ACQ). It has been proven that ACQ could be suppressed after confining the molecules into the MOF matrix.[23] In addition, the unique properties of MOFs, such as porosity and high surface area, will also make NIR materials exhibit possibility for their applications, *e.g.* in drug delivery and light-triggered treatment. Therefore, it is essential and urgent to develop organic linker-based NIR-MOFs and investigate their related applications in bioimaging and sensing.

The key procedure is how to design the linker structure to achieve extended light absorption and emission wavelength, and use them to prepare NIR-MOFs. Similar to benzo[1,2-*c*:4,5-*c*′]bis([1,2,5]thiadiazole), benzo[*c*][1,2,5]thiadiazole has also been proven to be an excellent acceptor group to synthesize donor–acceptor–donor (D–A–D) type organic linkers for constructing MOFs with tunable emission from deep blue to deep red.[24–29] In our previous work, we found that when much electron-deficient acceptor groups, compared with benzo[*c*][1,2,5]thiadiazole, were employed, such as naphtho[2,3-*c*][1,2,5]thiadiazole and naphtho[2,3-*c*][1,2,5]selenadiazole, a significant emission red-shift can be realized for resultant MOFs. For example, replacing benzo[*c*][1,2,5]thiadiazole in 4,4′-(benzo[*c*][1,2,5]thiadiazole-4,7-diyl)bis(3-methoxybenzoic acid) (H_2BTMB) with naphtho[2,3-*c*][1,2,5]selenadiazole to form 4,4′-(naphtho[2,3-*c*][1,2,5]selenadiazole-4,9-diyl) bis(3-methoxybenzoic acid) (H_2NSMB), a 117 nm red-shift is obtained from UiO-68-BTMB to UiO-68-NSMB (Fig. 1a, left).[23]

Besides, when increasing the electron density of donor groups, a remarkable bathochromic shift can also be achieved. For instance, replacing carboxylic acid-based donor groups in H_2BTMB with pyrazolate-based donor groups to form 4,7-di(1*H*-pyrazol-4-yl)benzo[*c*][1,2,5]thiadiazole (DPBT), a 42 nm bathochromic shift is realized from UiO-68-BTMB to HIAM-3004 (Fig. 1a, right). According to these studies, an emission library has been developed for LMOFs using benzo[*c*][1,2,5]thiadiazole and its analogue-based D–A–D type linkers with various donor and acceptor groups.[29] Therefore, we believe that NIR emissive organic linkers might be synthesized using donor groups with high electron density and acceptor groups possessing low electron density, which can be chosen from the built emission library.

To prove our hypothesis, one pyrazolate-based organic linker, 4,9-di(1*H*-pyrazol-4-yl)naphtho[2,3-*c*][1,2,5]selenadia-

Hoffmann Institute of Advanced Materials, Shenzhen Polytechnic, 7098 Liuxian Blvd, Nanshan District, Shenzhen 518055, P. R. China. E-mail: zhangjian@szpt.edu.cn, liuxiaoyuan1989@szpt.edu.cn

†Electronic supplementary information (ESI) available. CCDC 2278688. For ESI and crystallographic data in CIF or other electronic format see DOI: https://doi.org/10.1039/d3dt02134c

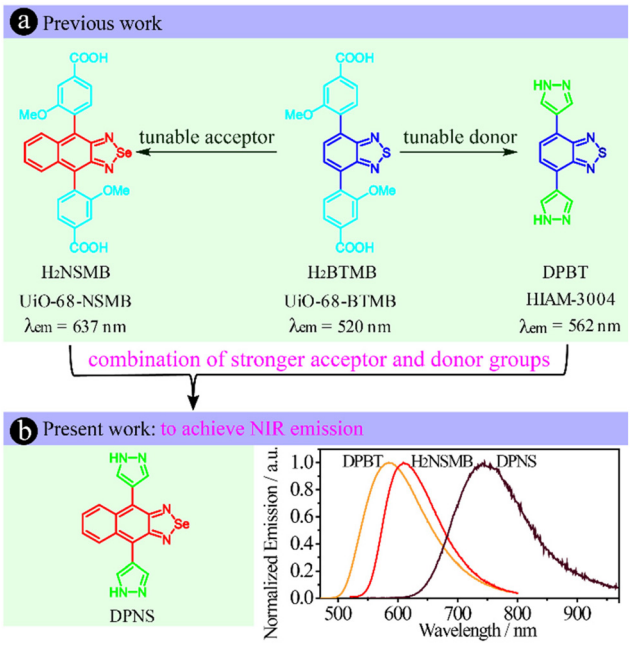

Fig. 1 (a) The schematic diagram illustrating the linker engineering strategy to prepare LMOFs with extended emission behaviours and (b) the proposed linker structure with near-infrared emission and the normalized emission spectra of DPBT, H_2NSMB and DPNS.

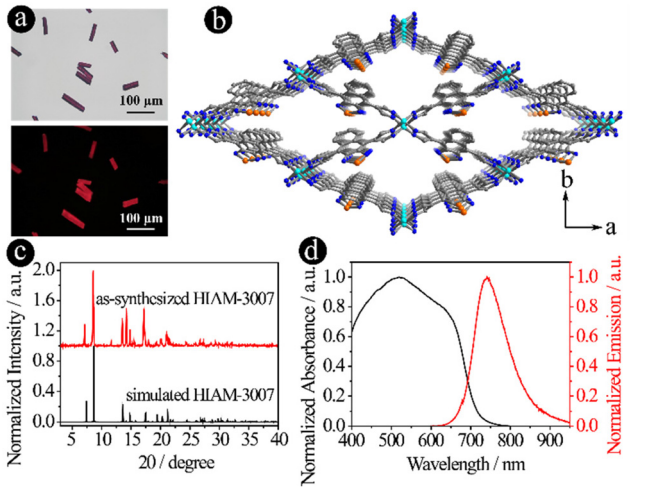

Fig. 2 (a) Single crystal images of HIAM-3007 under daylight (top) and 450 nm excitation (bottom); (b) single crystal structure of HIAM-3007 viewed along the *c* axis; (c) simulated and experimental PXRD patterns of HIAM-3007; and (d) solid-state UV-vis absorption and emission spectra of HIAM-3007.

zole (DPNS), was designed and synthesized (Fig. 1b, S1 and S2†). Then the steady-state emission spectrum of DPNS in *N*,*N*-dimethylformamide (DMF) solution was measured to confirm the hypothesis as shown in Fig. 1b. As expected, the maximum emission peak appears at 745 nm for DPNS, which is 136 and 160 nm red-shifted compared with that of DPBT and H_2NSMB. This result demonstrates that the combination of the donor group with stronger electron-donating properties and the acceptor group possessing decreased electron density into one organic linker indeed is a powerful approach for achieving NIR emission.

Then DPNS-based Zn-MOF, HIAM-3007 (HIAM = Hoffmann Institute of Advanced Materials, 30 = zinc), was synthesized according to our previous work. Typically HIAM-3007 is synthesized as follows: a 5 mL vial containing 29.7 mg Zn $(NO_3)_2{\cdot}6H_2O$, 36.5 mg DPNS, 1 mL DMF and 3 mL H_2O was placed in a preheated oven at 100 °C for 72 hours. Dark-red single crystals with deep-red emission were obtained (Fig. 2a). Single-crystal X-ray diffraction (sc-XRD) analysis reveals that HIAM-3007 crystallizes in the monoclinic crystal system with the C_2 space group. Each Zn^{2+} is coordinated in a tetrahedron geometry with four nitrogen atoms from four DPNS linkers. Each DPNS linker is coordinated with four Zn^{2+}, where each pyrazolate group connects two adjacent Zn^{2+}. The alternative connection of Zn^{2+} and pyrazolate groups form infinite chains along the *c* axis (Fig. 2b and S3†), which are further extended by the DPNS linkers to obtain the 3D structure. Hence, HIAM-3007 features a (4,4)-connected 3D porous network with ***pts*** topology as shown in Fig. S3,† which was the same as those reported for several bis(pyrazolate)-based MOFs.[30,31]

The phase purity of HIAM-3007 was confirmed by the excellent agreement between the simulated and experimental powder X-ray diffraction (PXRD) patterns (Fig. 2c). The thermogravimetric profile indicates that thermal stability of HIAM-3007 is up to 500 °C (Fig. S4†). Then the solid-state UV-vis absorption and emission spectra of HAIM-3007 were measured. As shown in Fig. 2d, the emission maxima at 741 nm was recorded with the emission tail towards 900 nm. The absorption spectrum of HIAM-3007 covers the whole visible-light range with an absorption edge close to 750 nm. These results indicate that NIR emissive MOFs can be constructed using D–A–D type organic linkers with stronger electron-donating donor and electron-withdrawing acceptor groups.

Nanosized HIAM-3007 was then prepared since it is essential to realize high dispensability of materials for aqueous phase-based chemical sensing. As shown in Fig. 3a, HIAM-3007 with a size less than 100 nm was obtained using triethylamine (TEA) as the modulator. It is interesting that the amount of TEA has no significant effect on the size of HIAM-3007 (Fig. S5†). The phase purity of nanosized HIAM-3007 was confirmed by PXRD (Fig. 3b and S6†). Then the chemical stability of nanosized HIAM-3007 was evaluated under different aqueous conditions to ensure its suitability for aqueous phase applications. As indicated by PXRD patterns shown in Fig. 3b, nanosized HIAM-3007 maintained its structural integrity after treatment in water, boiling water, pH = 4 and 12 solutions for 24 h, respectively, which is consistent with the previous works which showed that pyrazole-based MOFs possess excellent chemical stability in a wide range of pH conditions.[32–34] Almost no changes were observed for its emission behavior (Fig. 3c), size and morphology as confirmed by photoluminescence spectra and SEM (Fig. 3d and S7†).

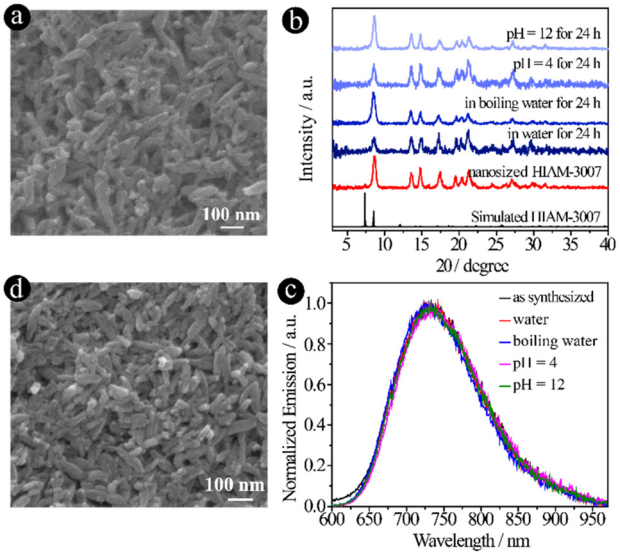

Fig. 3 (a) SEM images of nanosized HIAM-3007; (b) PXRD patterns of simulated, nanosized HIAM-3007 and after treatment under different conditions for 24 h; (c) aqueous phase emission spectra of HIAM-3007 after treatment under different conditions for 24 h; and (d) SEM images of nanosized HIAM-3007 after treatment in water for 24 h (scale bar: 100 nm).

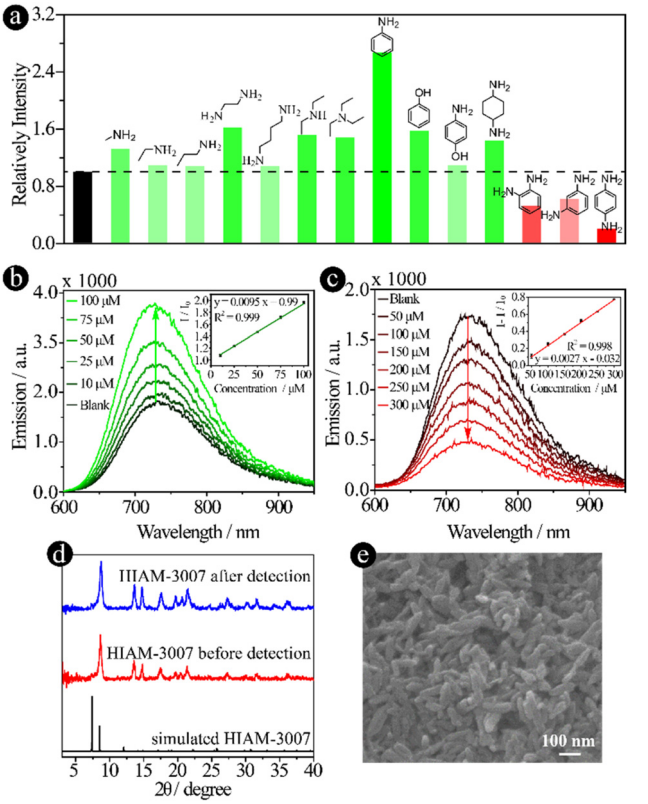

Fig. 4 (a) The selectivity test of nanosized HIAM-3007 toward different kinds of amines; concentration-dependent emission quenching of nanosized HIAM-3007 toward (b) aniline and (c) *p*-phenylenediamine; (d) the PXRD patterns of nanosized HIAM-3007 before and after detection of *p*-phenylenediamine; (e) the SEM images of nanosized HIAM-3007 after the detection of *p*-phenylenediamine.

These results demonstrate that nanosized HIAM-3007 is suitable for aqueous applications, such as chemical sensing.

Due to the great emission behaviour and excellent chemical stability of nanosized HIAM-3007, especially under aqueous conditions, its potential application as a chemical sensor was explored. As reported, benzo[*c*][1,2,5]thiadiazole and its derivative-based LMOFs exhibited unprecedented sensitivity towards amine detection;[26,35–38] different kinds of amines (aliphatic amines: methanamine, ethylamine, propylamine, ethylenediamine, 1,4-diaminobutane, diethylamine, triethylamine and 1,4-diaminocyclohexane; aromatic amines: aniline, *p*-aminophenol, *o*-phenylenediamine, *m*-phenylenediamine and *p*-phenylenediamine) were thus chosen to test the response of nanosized HIAM-3007.

As shown in Fig. 4a, varying degrees of emission enhancements were obtained for different kinds of aliphatic amines at a concentration of 300 μM, which is consistent with reported works which showed that turn-on detection of aliphatic amines can be obtained using benzo[*c*][1,2,5]thiadiazole and its derivative-based LMOFs.[26,35–37] These results can be ascribed to the strong interaction between aliphatic amines and naphtho[2,3-*c*][1,2,5]selenadiazole, which will restrict the motion of naphtho[2,3-*c*][1,2,5]selenadiazole, leading to reduced nonradiative recombination and enhanced emission.[26] The highest emission enhancement, 1.6 times compared with the blank sample, was recorded for diethylamine at a concentration of 300 μM, indicating that the sensitivity of HIAM-3007 for aliphatic amine detection is very low compared with the reported works.[26,36] However, it is interesting that, under the same test conditions, the highest emission enhancement of 2.64 times was achieved for aniline. A gradually increased emission was observed with increased concentration of aniline (Fig. 4b), where a good linear correlation coefficient of 0.999 was obtained at a concentration of 10 to 100 μM with a detection limit of 1.4 μM. The mechanism toward aniline can also be contributed to the fact that trapped anilines restrict the rotation of organic linkers through hydrogen bonding and π–π interaction.[39]

An 80% emission quenching was obtained for the detection of *p*-phenylenediamine at a concentration of 300 μM, which are 50% and 40% for detecting *o*-phenylenediamine and *m*-phenylenediamine under the same conditions. This result demonstrates that HIAM-3007 exhibits specific capacity for the detection of aromatic diamine, especially for *p*-phenylenediamine. Then the titration experiment was conducted to test the selectivity of HIAM-3007 toward *p*-phenylenediamine detection. The emission intensity of HIAM-3007 gradually decreased with an increased concentration of *p*-phenylenediamine (Fig. 4c). A good linear correlation coefficient of 0.998 was calculated for the detection of *p*-phenylenediamine with a detection limit of 5.2 μM.

To further confirm the opposite responses of nanosized HIAM-3007 towards aniline and *p*-phenylenediamine, the fluo-

rescence lifetimes of HIAM-3007 before and after the addition of these two compounds were recorded (Fig. S8†). The lifetimes are 0.27, 0.42 and 0.19 ns for pristine nanosized HIAM-3007, nanosized HIAM-3007 with aniline and *p*-phenylenediamine, respectively, which are consistent with the emission enhancement and quenching enhancement upon addition of aniline and *p*-phenylenediamine to the suspension of nanosized HIAM-3007. Due to the high chemical stability of nanosized HIAM-3007, the emission responses of HIAM-3007 towards aniline and *p*-phenylenediamine at pH = 4 and pH = 10 were further investigated. Interestingly, in pH = 10 aqueous solutions, aniline and *p*-phenylenediamine exhibited similar responses to those shown in Fig. 2b and c under pH = 7 conditions, while under pH = 4 conditions, slight responses were recorded (Fig. S9†). As mentioned above, the response mechanism was attributed to hydrogen bonding and π–π interaction. Thus, in aqueous solutions, the abundant H^+/OH^- might limit the formation of hydrogen bonds, which could influence the detection performance of HIAM-3007 towards aniline and *p*-phenylenediamine.

These aforementioned results demonstrated that nanosized HIAM-3007 exhibits high selectivity and sensitivity for emission turn-off detection of *p*-phenylenediamine. The almost identical PXRD patterns and SEM images of HIAM-3007 before and after detection indicated its high chemical stability (Fig. 4d and e), revealing that nanosized HIAM-3007 has great potential for practical application as a chemical sensor.

In conclusion, a new Zn-MOF, HIAM-3007, with near-infrared-I emissive behaviour (λ_{em} > 740 nm in the solid state) was constructed by using a pyrazolate and naphtho[2,3-*c*][1,2,5]selenadiazole based donor–acceptor–donor type organic linker. Nanosized HIAM-3007 shows excellent chemical stability and was used for aniline and *p*-phenylenediamine detection with high selectivity and sensitivity. This work provides a practical route to the rational design of organic linkers for preparing MOFs with near-infrared emission.

Conflicts of interest

There are no conflicts to declare.

Acknowledgements

The authors gratefully acknowledge the support from Shenzhen Polytechnic. H.-L. Xia acknowledges the financial support from the Shenzhen Science and Technology Program (RCBS20221008093232044). X.-Y. Liu acknowledges the financial support from the National Natural Science Foundation of China (No. 22201185), the Guangdong Basic and Applied Basic Research Foundation (2023A1515011494), and start-up funding for Shenzhen High-Caliber Personnel of Shenzhen Polytechnic (6022310053K).

References

1 Q. Gong, Z. Hu, B. J. Deibert, T. J. Emge, S. J. Teat, D. Banerjee, B. Mussman, N. D. Rudd and J. Li, *J. Am. Chem. Soc.*, 2014, **136**, 16724–16727.
2 J. Cornelio, T.-Y. Zhou, A. Alkaş and S. G. Telfer, *J. Am. Chem. Soc.*, 2018, **140**, 15470–15476.
3 W. J. Newsome, S. Ayad, J. Cordova, E. W. Reinheimer, A. D. Campiglia, J. K. Harper, K. Hanson and F. J. Uribe-Romo, *J. Am. Chem. Soc.*, 2019, 11298–11303.
4 X.-Y. Liu, W. P. Lustig and J. Li, *ACS Energy Lett.*, 2020, **5**, 2671–2680.
5 G. Han, S. Wu, K. Zhou, H.-L. Xia, X.-Y. Liu and J. Li, *Inorg. Chem.*, 2022, **61**, 3363–3367.
6 J. Li, S. Yuan, J.-S. Qin, J. Pang, P. Zhang, Y. Zhang, Y. Huang, H. F. Drake, W. R. Liu and H.-C. Zhou, *Angew. Chem., Int. Ed.*, 2020, **59**, 9319–9323.
7 Z. Hu, B. J. Deibert and J. Li, *Chem. Soc. Rev.*, 2014, **43**, 5815–5840.
8 Y. Cui, B. Li, H. He, W. Zhou, B. Chen and G. Qian, *Acc. Chem. Res.*, 2016, **49**, 483–493.
9 W. P. Lustig, S. Mukherjee, N. D. Rudd, A. V. Desai, J. Li and S. K. Ghosh, *Chem. Soc. Rev.*, 2017, **46**, 3242–3285.
10 L. Chen, J.-W. Ye, H.-P. Wang, M. Pan, S.-Y. Yin, Z.-W. Wei, L.-Y. Zhang, K. Wu, Y.-N. Fan and C.-Y. Su, *Nat. Commun.*, 2017, **8**, 15985.
11 J. Qiao, X. Liu, L. Zhang, J. F. Eubank, X. Liu and Y. Liu, *J. Am. Chem. Soc.*, 2022, **144**, 17054–17063.
12 B. Wang, P. Wang, L.-H. Xie, R.-B. Lin, J. Lv, J.-R. Li and B. Chen, *Nat. Commun.*, 2019, **10**, 3861.
13 J. Park, Q. Jiang, D. Feng, L. Mao and H. C. Zhou, *J. Am. Chem. Soc.*, 2016, **138**, 3518–3525.
14 J. Park, M. Xu, F. Li and H. C. Zhou, *J. Am. Chem. Soc.*, 2018, **140**, 5493–5499.
15 B. Li, X. Lu, Y. Tian and D. Li, *Angew. Chem., Int. Ed.*, 2022, **61**, e202206755.
16 S. A. A. Razavi and A. Morsali, *Coord. Chem. Rev.*, 2019, **399**, 213023.
17 A. L. Antaris, H. Chen, K. Cheng, Y. Sun, G. Hong, C. Qu, S. Diao, Z. Deng, X. Hu, B. Zhang, X. Zhang, O. K. Yaghi, Z. R. Alamparambil, X. Hong, Z. Cheng and H. Dai, *Nat. Mater.*, 2016, **15**, 235–242.
18 B. Li, M. Zhao and F. Zhang, *ACS Mater. Lett.*, 2020, **2**, 905–917.
19 S. Liu, Y. Li, R. T. K. Kwok, J. W. Y. Lam and B. Z. Tang, *Chem. Sci.*, 2020, **12**, 3427–3436.
20 Z. Lei and F. Zhang, *Angew. Chem., Int. Ed.*, 2021, **60**, 16294–16308.
21 W. Xu, D. Wang and B. Z. Tang, *Angew. Chem., Int. Ed.*, 2021, **60**, 7476–7487.
22 H. Shen, F. Sun, X. Zhu, J. Zhang, X. Ou, J. Zhang, C. Xu, H. H. Y. Sung, I. D. Williams, S. Chen, R. T. K. Kwok, J. W. Y. Lam, J. Sun, F. Zhang and B. Z. Tang, *J. Am. Chem. Soc.*, 2022, **144**, 15391–15402.
23 S. Wu, D. Ren, K. Zhou, H. L. Xia, X. Y. Liu, X. Wang and J. Li, *J. Am. Chem. Soc.*, 2021, **143**, 10547–10552.

24 R. J. Marshall, Y. Kalinovskyy, S. L. Griffin, C. Wilson, B. A. Blight and R. S. Forgan, *J. Am. Chem. Soc.*, 2017, **139**, 6253–6260.
25 E. Angioni, R. J. Marshall, N. J. Findlay, J. Bruckbauer, B. Breig, D. J. Wallis, R. W. Martin, R. S. Forgan and P. J. Skabara, *J. Mater. Chem. C*, 2019, **7**, 2394–2400.
26 A. Mallick, A. M. El-Zohry, O. Shekhah, J. Yin, J. Jia, H. Aggarwal, A. H. Emwas, O. F. Mohammed and M. Eddaoudi, *J. Am. Chem. Soc.*, 2019, **141**, 7245–7249.
27 D. Ren, H.-L. Xia, K. Zhou, S. Wu, X.-Y. Liu, X. Wang and J. Li, *Angew. Chem., Int. Ed.*, 2021, **60**, 25048–25054.
28 H.-L. Xia, K. Zhou, J. Guo, J. Zhang, X. Huang, D. Luo, X.-Y. Liu and J. Li, *Chem. Sci.*, 2022, **13**, 9321–9328.
29 H.-L. Xia, K. Zhou, S. Wu, D. Ren, K. Xing, J. Guo, X. Wang, X.-Y. Liu and J. Li, *Chem. Sci.*, 2022, **13**, 8036–8044.
30 N. Mosca, R. Vismara, J. A. Fernandes, S. Casassa, K. V. Domasevitch, E. Bailón-García, F. J. Maldonado-Hódar, C. Pettinari and S. Galli, *Cryst. Growth Des.*, 2017, **17**, 3854–3867.
31 C. Pettinari, A. Tăbăcaru and S. Galli, *Coord. Chem. Rev.*, 2016, **307**, 1–31.
32 T. He, X.-J. Kong and J.-R. Li, *Acc. Chem. Res.*, 2021, **54**, 3083–3094.
33 S. Yuan, L. Feng, K. Wang, J. Pang, M. Bosch, C. Lollar, Y. Sun, J. Qin, X. Yang, P. Zhang, Q. Wang, L. Zou, Y. Zhang, L. Zhang, Y. Fang, J. Li and H. C. Zhou, *Adv. Mater.*, 2018, **30**, e1704303.
34 M. Ding, X. Cai and H. L. Jiang, *Chem. Sci.*, 2019, **10**, 10209–10230.
35 D. I. Pavlov, T. S. Sukhikh, A. A. Ryadun, V. V. Matveevskaya, K. A. Kovalenko, E. Benassi, V. P. Fedin and A. S. Potapov, *J. Mater. Chem. C*, 2022, **10**, 5567–5575.
36 Y.-M. Wang, C. Liu, H. Zhi, X. Zhang, Y. Xu, Y. Wang, R. Yang and X.-B. Yin, *Chem. Eng. J.*, 2022, **441**, 136049.
37 P.-M. Chuang, Y.-J. Tu and J.-Y. Wu, *Sens. Actuators, B*, 2022, **366**, 131967.
38 W.-Q. Zhang, Q.-Y. Li, J.-Y. Cheng, K. Cheng, X. Yang, Y. Li, X. Zhao and X.-J. Wang, *ACS Appl. Mater. Interfaces*, 2017, **9**, 31352–31356.
39 B. Wang, R. He, L.-H. Xie, Z.-J. Lin, X. Zhang, J. Wang, H. Huang, Z. Zhang, K. S. Schanze, J. Zhang, S. Xiang and B. Chen, *J. Am. Chem. Soc.*, 2020, **142**, 12478–12485.